LUND UNIVERSITY

Effective Charges Near 56Ni and Production of Anti-Nuclei Studied with Heavy-Ion Reactions

du Rietz, Rickard

2005

Paper III

Effective Charges in the fp Shell

R. du Rietz,[1] J. Ekman,[1] D. Rudolph,[1] C. Fahlander,[1] A. Dewald,[2] O. Möller,[2] B. Saha,[2] M. Axiotis,[3] M. A. Bentley,[4] C. Chandler,[4] G. de Angelis,[3] F. Della Vedova,[5] A. Gadea,[3] G. Hammond,[4] S. M. Lenzi,[5] N. Mărginean,[3] D. R. Napoli,[3] M. Nespolo,[5] C. Rusu,[3] and D. Tonev[3]

[1]*Department of Physics, Lund University, S-22100 Lund, Sweden*
[2]*Institut für Kernphysik der Universität zu Köln, D-50937 Köln, Germany*
[3]*Instituto Nazionale di Fisica Nucleare, Laboratori Nazionali di Legnaro, I-35020 Legnaro, Italy*
[4]*School of Chemistry and Physics, Keele University, Keele, Staffordshire ST5 5BG, United Kingdom*
[5]*Dipartimento di Fisica dell'Università and INFN, Sezione di Padova, I-35141 Padova, Italy*

(Received 16 August 2004; published 22 November 2004)

Following the heavy-ion fusion-evaporation reaction $^{32}S + ^{24}Mg$ at 95 MeV beam energy the lifetimes of analogue states in the $T_z = \pm 1/2$ $A = 51$ mirror nuclei ^{51}Fe and ^{51}Mn have been measured using the Cologne plunger device coupled to the GASP γ-ray spectrometer. The deduced $B(E2; 27/2^- \rightarrow 23/2^-)$ values afford a unique opportunity to probe isoscalar and isovector polarization charges and to derive effective proton and neutron charges, ε_p and ε_n, in the fp shell. A comparison between the experimental results and several different large-scale shell-model calculations yields $\varepsilon_p \sim 1.15e$ and $\varepsilon_n \sim 0.80e$.

DOI: 10.1103/PhysRevLett.93.222501 PACS numbers: 21.10.Tg, 21.60.Cs, 27.40.+z

In the isospin formalism the proton and neutron are treated as two different quantum states of the same particle, the nucleon. The assumption of isospin symmetry relies on the fact that the nucleon-nucleon interaction is charge independent. In reality, however, the symmetry is broken by the Coulomb force between protons [1].

Nuclei in the vicinity of the doubly magic $N = Z$ nuclei ^{40}Ca and ^{56}Ni as well as $N \sim Z$ nuclei near the middle of the $1f_{7/2}$ shell are well described by large-scale shell-model calculations [2]. They are well suited for isospin symmetry studies since the $1f_{7/2}$ shell is relatively isolated in energy. Together with significant theoretical effort the understanding and interpretation of Coulomb effects in mirror nuclei, which are pairs of nuclei with the number of protons and neutrons interchanged, has increased substantially during recent years [3–5]. However, almost all studies so far have been limited to the comparison of excitation energies in so called Mirror Energy Difference diagrams. Other spectroscopic quantities, such as lifetimes of excited states and related electromagnetic properties of mirror nuclei, have only recently been looked upon [6].

Electromagnetic properties of nuclei give information on core polarization effects due to the valence particles outside closed shells, if the configurations of the valence particles are taken care of by large-scale shell-model calculations. In practice, the polarization effects are accounted for in nuclear models by using effective nucleon charges and gyromagnetic factors instead of those of the bare nucleons. The polarization charge, which is the difference between the effective and bare charge, is believed to arise from virtual excitations of isoscalar and isovector giant resonances of the nucleus. As the wave functions of analogue states in mirror nuclei are to first order identical under the exchange of protons and neutrons, the study of mirror nuclei offers a unique opportunity to access, probe, and pin down the effective charges.

The $A = 51$ mirror nuclei ^{51}Fe and ^{51}Mn have well established level schemes [7–9], which are shown in Fig. 1. The lifetimes of the nanosecond isomeric $17/2^-$ states are known in both nuclei, and a lifetime of $\tau = 130(25)$ ps has been suggested for the terminating $27/2^-$ state in ^{51}Mn [10]. In this Letter, we present a refined number for this state and the first measurement of the lifetime of its analogue state in ^{51}Fe. A unique study, based on large-scale shell-model calculations, is performed and for the first time a quantitative estimate of effective charges near ^{56}Ni is derived.

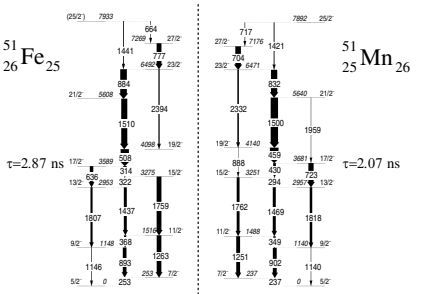

FIG. 1. Level schemes of the $A = 51$ mirror nuclei [7–9]. Energy labels are in keV and the widths of the arrows correspond to the relative intensities of the transitions.

The experiment was performed at the Legnaro National Laboratory using the heavy-ion fusion-evaporation reaction $^{32}S + ^{24}Mg$ with a beam energy of 95 MeV. The 99.92% isotopically enriched and on average 0.95 mg/cm^2 thick ^{24}Mg target was mounted inside the Cologne plunger device [11] in front of a stretched 13 mg/cm^2 gold stopper foil. Data were taken at 21 target-stopper distances ranging from electric contact to 4.0 mm.

The mass $A = 51$ mirror nuclei ^{51}Fe and ^{51}Mn were produced via the evaporation of one α particle and one neutron ($1\alpha 1n$ channel) and one α particle and one proton ($1\alpha 1p$ channel), respectively. The γ rays were detected with the GASP detector array [12] using its 40 HPGe detectors (distributed in seven rings at 34.6°, 59.4°, 72.0°, 90.0°, 108.0°, 120.6°, and 145.4°) and 74 BGO elements. Events with at least one BGO element and two HPGe detectors firing in coincidence were accepted by the event trigger. At the end of the experiment, ^{56}Co, ^{133}Ba, and ^{152}Eu standard sources were used to calibrate the detector system.

The method used to determine the lifetimes of the $27/2^-$ states in the $A = 51$ mirror pair is based on very specific features of their decay schemes. They consist of essentially three regimes: the transitions below the isomeric $17/2^-$ states, those feeding into the long-lived (~100 ps) $27/2^-$ states, and the short-lived states in between (see Fig. 1). Thus it is possible to apply the recoil distance Doppler shift (RDDS) method to the 777 and 704 keV (or 884 and 832 keV) transitions in spectra taken in coincidence with low-lying transitions, which are essentially always emitted from stopped residues.

Therefore, for each distance the events were sorted offline into $\gamma\gamma$ coincidence matrices with γ rays detected in one given detector ring placed along one axis and γ rays detected anywhere in the array along the second axis of the matrix. Clean spectra of ^{51}Fe and ^{51}Mn are shown in Fig. 2. They are obtained by gating on the low-energy 253 and 237 keV $7/2^- \rightarrow 5/2^-$ transitions, respectively. A RDDS analysis is performed using the two most forward and the two most backward detector rings of GASP, where the shifted and unshifted components of the coincident transitions are well separated.

The analysis of the same transition for different distances requires a normalization of its intensity due to, e.g., different beam currents or measuring times. To obtain these normalization coefficients for each distance, the intensities of the unshifted and Doppler shifted components for the 459 and 832 keV transitions observed in all detector rings were summed up in spectra in coincidence with the 237 keV ground-state transition in ^{51}Mn. The (mainly systematic) uncertainty for the normalization coefficients was estimated to be 2%.

The normalization coefficients are also used as weighting factors when different measurements at about the same distance were combined. This is necessary for the analysis of the transitions from the very weakly populated nucleus ^{51}Fe. For each of the 21 target-distance combinations the recoil velocity was derived from the positions of the stopped and Doppler shifted components of the intense 1500 keV $21/2^- \rightarrow 19/2^-$ transition in ^{51}Mn. The velocities range from 3.7% to 4.1% of the speed of light for the three different targets used during the experiment. Using these velocities the 21 distances can be converted into 21 flight times, which are then combined in nine effective flight times used in the analysis: 0.537(7), 1.45(1), 3.42(5), 10.3(2), 34.8(9), 61.2(14), 105(3), 175(5), and 354(9) ps.

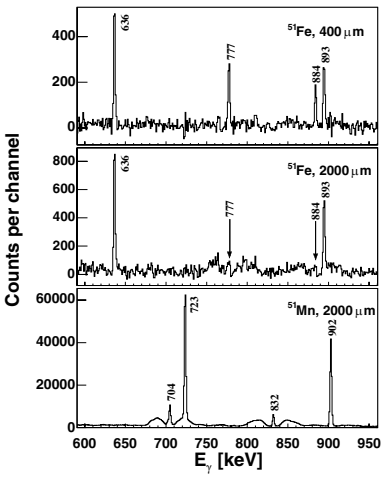

FIG. 2. Gamma-ray spectra taken at different distances in the GASP detector rings at 34.6°, 59.4°, 120.6°, and 145.4°. They are in coincidence with the $7/2^- \rightarrow 5/2^-$ 253 keV transition in ^{51}Fe (top, middle) and the 237 keV mirror transition in ^{51}Mn (bottom). Energy labels of the peaks are in keV. Note the significant reduction of statistics when moving from ^{51}Mn to the more exotic isotope ^{51}Fe.

The top two spectra of Fig. 2 illustrate how the target-stopper distance affects the intensities of the stopped and Doppler shifted components. For the short distance (400 μm) the four transitions at 636, 777, 884, and 893 keV in ^{51}Fe are clearly seen as stopped peaks. When increasing the distance to 2000 μm the stopped components of the two transitions at 777 and 884 keV are significantly reduced and Doppler shifted and broadened peaks arise on each side of the stopped peaks. The 636 and 893 keV transitions are still observed as stopped peaks, because they are situated below the isomeric $17/2^-$ state and the flight distance is still rather short with respect to its lifetime.

The comparison of the ^{51}Fe and ^{51}Mn spectra for the same distance in Fig. 2 shows a difference in statistics of some 2 orders of magnitude. The large amount of statistics in the ^{51}Mn spectrum allows us to discriminate Doppler shifted components even for the transitions below the $17/2^-$ state (723 and 902 keV). Additionally, it enables both a thorough investigation of possible systematic errors and a proper normalization in the course of the analysis.

Figure 3 illustrates the decay curves of the 777 keV $27/2^- \rightarrow 23/2^-$ transition in ^{51}Fe and the $23/2^- \rightarrow 21/2^-$ 832 keV transition in ^{51}Mn. The analysis of the $27/2^- \rightarrow 23/2^-$ 704 keV transition was hampered due to Doppler shifted components of the 723 keV $17/2^- \rightarrow 13/2^-$ and 717 keV $25/2^- \rightarrow 27/2^-$ transitions (cf. Figure 2) as well as background radiation at 701 keV from the decay of the $19/2^-$ isomer in ^{53}Fe. To account for possible side feeding (<10%) directly into the $23/2^-$ state, the decay curve of the 832 keV line was least-squares fitted with a short ($\tau < 10$ ps) and a long lifetime component. The result is $\tau = 100.7 \pm 1.2 \pm 3$ ps for the $27/2^-$ state in ^{51}Mn, i.e., $B(E2) = 46.7(14)\ e^2\,\mathrm{fm}^4$. The systematic uncertainty of ± 3 ps is related to the normalization, the exact determination of the yield of the stopped component at large distances, possible short-lived ($\tau < 1$ ps cf. [9]) feeding into the $27/2^-$ state, and combining the yields of measurements at several distances.

To increase statistics in the case of ^{51}Fe, spectra in coincidence with the 253, 314, and 636 keV transitions from the two most forward and the two most backward detector rings were summed. Since a stopped component of the 777 keV line was absent in the spectrum taken at the largest distance, it was excluded from the analysis. The resulting lifetime of the $27/2^-$ state in ^{51}Fe is found to be $\tau = 69.7 \pm 1.6 \pm 3$ ps, i.e., $B(E2) = 41.3(24)\ e^2\,\mathrm{fm}^4$. The ratio, R, between the $B(E2)$ values of the mirror transitions in ^{51}Fe and ^{51}Mn amounts to $R = 0.884(22)$.

To study the consequences of the lifetime results on polarization and effective charges, large-scale shell-model calculations were performed using the shell-model code ANTOINE [13,14]. The calculations employ the full fp space containing the $1f_{7/2}$ orbit below and the $2p_{3/2}$, $1f_{5/2}$, and $2p_{1/2}$ orbits above the $N, Z = 28$ shell closure. The configuration space was truncated to allow for excitations of up to five particles across the shell closure. This configuration space provides predictions more or less indistinguishable from calculations using the full fp space [2]. Three interactions have been studied: The standard KB3G interaction without any Coulomb interaction, with theoretical harmonic-oscillator Coulomb matrix elements (Coulomb HO), and with the $1f_{7/2}$ Coulomb matrix elements replaced with the experimental values from the $A = 42$ mirror pair (Coulomb A42).

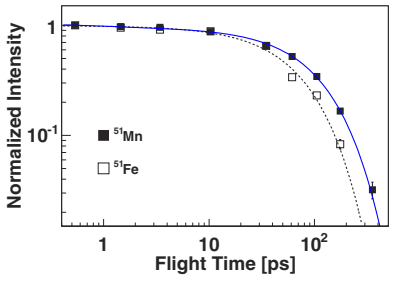

FIG. 3 (color online). Decay curves for the 832 keV transition in ^{51}Mn (solid line) and the 777 keV transition in ^{51}Fe (dashed line) for nine effective flight distances.

The predicted reduced $E2$-transition probabilities are generally expressed as a sum over all nucleons,

$$B(E2; J_i \rightarrow J_f) = \frac{1}{2J_i + 1} \left| \left\langle J_f \right| \left| \sum_{i=1}^{A} \varepsilon_i r^2 Y_{20} \right| \left| J_i \right\rangle \right|^2, \quad (1)$$

where ε_i denote the effective nucleon charges and $\langle r^2 \rangle = b_0^2 A^{1/3}(N + 3/2)$ in the case of harmonic-oscillator wave functions. Note that the principle quantum number N and thus $\langle r^2 \rangle$ is constant within the fp shell. The harmonic-oscillator parameter, b_0, is commonly set to 1.01.

The effective proton and neutron charges, ε_p and ε_n, are introduced to account for polarization effects of the valence nucleons on the otherwise inert core of the shell-model calculation. The isoscalar and isovector polarization charges, $e_{\mathrm{pol}}^{(0)}$ and $e_{\mathrm{pol}}^{(1)}$, arise from the virtual excitation of the isoscalar and isovector giant quadrupole resonances (GQR) of the core. Thus,

$$\varepsilon_p = 1 + e_{\mathrm{pol}}^{(0)} - e_{\mathrm{pol}}^{(1)}, \qquad \varepsilon_n = e_{\mathrm{pol}}^{(0)} + e_{\mathrm{pol}}^{(1)}, \quad (2)$$

where it is predicted that $e_{\mathrm{pol}}^{(0)} = Z/A \sim 0.5$ and $e_{\mathrm{pol}}^{(1)} \sim 0.32$ in the case of $N \sim Z$ nuclei [15].

In the absence of Coulomb effects, the wave functions of analogue states are identical with respect to the exchange of protons and neutrons. Therefore, the $B(E2)$ values of mirror transitions and their ratio are sensitive to the effective charges according to Eq. (1) and, consequently, to the isovector polarization charge [cf. Eq. (2)].

Assuming identical orbital radii, i.e., the same b_0 for ^{51}Mn and ^{51}Fe, the $B(E2)$ values for the two $27/2^- \rightarrow 23/2^-$ transitions were calculated. The experimental values and their ratio are reproduced simultaneously for different combinations of the three parameters b_0 and the isoscalar and isovector polarization charges. Figure 4 illustrates this dependency for two different sets of Coulomb matrix elements and one set without any Coulomb interaction. Table I summarizes the results for $b_0 = 1.01$. The uncertainties in $e_{\mathrm{pol}}^{(0)}$ and $e_{\mathrm{pol}}^{(1)}$ are determined by reproducing the maximum (minimum)

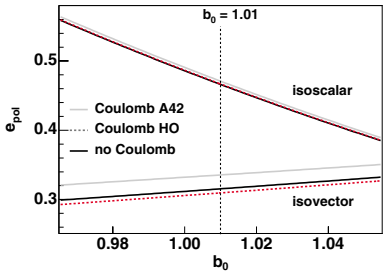

FIG. 4 (color online). Polarization charges, necessary to reproduce the $B(E2; 27/2^- \rightarrow 23/2^-)$ values in the $A = 51$ mirror nuclei, as a function of b_0 for three different shell-model calculations. The top three lines correspond to the isoscalar component, $e^{(0)}_{\mathrm{pol}}$, while the bottom three lines represent the isovector component, $e^{(1)}_{\mathrm{pol}}$.

$B(E2; 27/2^- \rightarrow 23/2^-)$ value in ^{51}Mn and the minimum (maximum) $B(E2; 27/2^- \rightarrow 23/2^-)$ value in ^{51}Fe, respectively. It is intriguing that the numbers in Table I result in effective charges similar to recently refined estimates in the ^{100}Sn region (cf. Ref. [16], and references therein). Most interestingly, however, is that the present results are in very good agreement with Eq. 6-386b in Ref. [15], where the effective charge phenomenon is treated as a weak coupling of the valence nucleons to the GQR of the core. This coupling gives rise to a mixing of the GQR components into the shell-model states, which results in an increase of the transition matrix elements. The isoscalar and isovector GQRs originate from the particle-hole states with excitation energies of about $2\hbar\omega_0 \sim 22$ MeV for $A = 51$.

From Fig. 4 it is seen that the isoscalar $e^{(0)}_{\mathrm{pol}}$ component is much more sensitive to changes in nuclear radii than the isovector $e^{(1)}_{\mathrm{pol}}$ component. In turn, the isoscalar part is rather independent of the choice of $1f_{7/2}$ Coulomb matrix elements, whereas the isovector part shows a more pronounced dependence. It is interesting to note that the $e^{(1)}_{\mathrm{pol}}$ results obtained using the two sets of Coulomb matrix elements are situated on opposite sides of the line originating from the calculation without any Coulomb interaction. The major differences between the two sets are the $1f_{7/2}$ $J = 2$ and $1f_{7/2}$ $J = 6$ Coulomb matrix elements. A detailed investigation reveals that mainly the latter is responsible for this effect.

The effective charges given above are extracted under the assumption that the radii of the two mirror partners are identical (b_0 is the same for both members). However, it is reasonable to assume that the Coulomb interaction pushes the proton wave functions towards larger radii with respect to the neutron wave functions. Following this argument, the radius of ^{51}Fe should be slightly larger than the radius of ^{51}Mn. But, since this adds extra degrees of freedom, more experimental data are required.

TABLE I. Isoscalar and isovector polarization charges, which simultaneously reproduce the $B(E2; 27/2^- \rightarrow 23/2^-)$ values in the $A = 51$ mirror nuclei, for three different shell-model calculations using $b_0 = 1.01$.

	No Coulomb	Coulomb HO	Coulomb A42
$e^{(0)}_{\mathrm{pol}}$	0.466(3)	0.466(3)	0.471(2)
$e^{(1)}_{\mathrm{pol}}$	0.316(26)	0.310(37)	0.336(37)

In summary, the lifetimes of the $27/2^-$ states in the $A = 51$ mirror nuclei have been measured. Utilizing the results provides an unique way to investigate the effective charges near ^{56}Ni. A detailed comparison with large-scale shell-model calculations gives effective charges of $\varepsilon_n \sim 0.80$ and $\varepsilon_p \sim 1.15$ for the neutron and proton, respectively.

We would like to express our gratitude to I. Hamamoto for valuable discussions. We thank the accelerator crew at LNL for the excellent support. This research was supported in part by the Swedish Research Council, the European Commission under Contract No. HPRI-1999-CT-00083, and the European Community programme IHP under Contract No. HPMF-CT-2002-02018.

[1] *Isospin in Nuclear Physics*, edited by D. H. Wilkinson (North-Holland Publishing Company, Amsterdam, 1969).
[2] A. Poves, J. Sanchez-Solano, E. Caurier, and F. Nowacki, Nucl. Phys. **A694**, 157 (2001).
[3] A. P. Zuker *et al.*, Phys. Rev. Lett. **89**, 142502 (2002).
[4] S. J. Williams, Ph.D. thesis, Keele University, 2003 (unpublished).
[5] J. Ekman, Ph.D. thesis, Lund University, 2004, ISBN 91-628-6061-5.
[6] D. Tonev *et al.*, Phys. Rev. C **65**, 034314 (2002).
[7] M. A. Bentley *et al.*, Phys. Rev. C **62**, 051303(R) (2000).
[8] J. Ekman *et al.*, Eur. Phys. J. A **9**, 13 (2000).
[9] J. Ekman *et al.*, Phys. Rev. C **70**, 014306 (2004).
[10] J. W. Noe and P. Gural, *Proceedings of the International Conference on Medium-Light Nuclei, Florence, Italy, 1978*, edited by P. Blasi and R. A. Ricci (Editrice Compositori, Bologna, 1978), p. 459.
[11] A. Dewald *et al.*, Nucl. Phys. **A545**, 822 (1992).
[12] C. Rossi Alvarez, Nucl. Phys. News **3**, 3 (1993).
[13] E. Caurier, shell-model code ANTOINE, IRES, Strasbourg, 1989.
[14] E. Caurier and F. Nowacki, Acta Phys. Pol. **30**, 705 (1999).
[15] A. Bohr and B. R. Mottelson, *Nuclear Structure* (Benjamin Inc., New York, 1975), Vol. 2, Chap. 6.
[16] A. Blazhev *et al.*, Phys. Rev. C **69**, 064304 (2004).